AIAA Propulsion and Energy Forum
19-22 August 2019, Indianapolis, IN
AIAA Propulsion and Energy 2019 Forum

10.2514/6.2019-4465

Aircraft Conceptual Design Including Powertrain System Architecture and Distributed Propulsion

F. Orefice[1], P. Della Vecchia[2], D. Ciliberti[3], and F. Nicolosi[4]
University of Naples "Federico II", Naples, 80125, Italy

The paper presents a thorough conceptual design approach for a generic aircraft with conventional, hybrid-electric, or full-electric powertrain. It follows the steps of classic aircraft design methods, including the main aspects related to the hybridization of an aircraft: powertrain architectures, energy sources, aerodynamic-propulsive interactions, stability and control effects. Such aircraft is designed considering design and regulations requirements. Three are the main steps of the conceptual design approach presented: preliminary design, sizing, and analysis. The first step provides a statistical baseline, including both geometry and weight breakdown, moving from top-level requirements. The sizing activity provides the energetic requirements and the mass breakdown, by combining the free choice of the designer with aviation regulations and requirements. The subsequent analysis aims to choose the baseline for high-fidelity optimization. The first application of the presented workflow deals with regional turboprop aircraft and it is based on the ATR-42 design mission. However, in the present work, a further investigation of the possible concepts, based on different design missions, highlights that the competitiveness of hybrid-electric aircrafts cannot be based on the same mission profiles on which nowadays aircrafts have been designed.

I. Nomenclature

$(\cdot)_1$	=	subscript for primary propulsive system
$(\cdot)_2$	=	subscript for secondary propulsive system
$C_{(\cdot)}$	=	aerodynamic coefficient
E	=	energy
P	=	power
S	=	wing planform area
W	=	weight
A_s	=	cross-sectional area of the slipstream
A_p	=	area of the disk propeller
T	=	thrust
$V_{(\cdot)}$	=	velocity at the location $(\cdot)$
$a_{(\cdot)}$	=	axial induction at the location $(\cdot)$
φ	=	shaft power ratio
Φ	=	supplied power ratio
η	=	efficiency
χ	=	thrust hybridization factor
DEP	=	Distributed Electric Propulsion
DOC	=	Direct Operative Costs
PMAD	=	Power Management And Distribution
TLAR	=	Top Level Aircraft Requirements

II. Challenges to the conceptual design process of a (hybrid) electric aircraft

The present work aims to define a single conceptual design process for conventional, hybrid-electric, and full-electric aircraft, developing a dedicated tool, also underlying the critical points and the major advantages resulting from different powertrain architectures. Attention is given to the regional turboprop aircraft (ATR-42) category, as main example of this conceptual design process. Comparisons will be made in order to point out differences in fuel consumption, propulsive and aerodynamic efficiencies, as well as weight breakdown among conventional, turboelectric, and hybrid-electric architectures. The importance of hybrid-

[1] PhD Student, DAF Research Group, Dept. of Industrial Engineering, AIAA Student Member.
[2] Assistant Professor, DAF Research Group, Dept. of Industrial Engineering, AIAA Member.
[3] Assistant Professor, DAF Research Group, Dept. of Industrial Engineering.
[4] Associate Professor, DAF Research Group, Dept. of Industrial Engineering, AIAA Member.

electric aircraft capable of competing in terms of performance and market share has already been stressed with the ATR-42 and ATR-72 airplanes [1,2]. However, by using current technology (battery, electric motors, etc.), there will not be any advantage from the use of hybrid-electric powertrain for such airplane category. Therefore, many authors rely on technological trends, sometimes with optimistic projections [1,3,4]. The present work will maintain a conservative attitude, while trying to exploit the aircraft concept and the mission profile to reduce the gap between the current turboprop performance and the advanced powertrain turboprop generation.

Recently, some methods to perform a conceptual design of hybrid-electric or pure electric aircraft have been published, although not consolidated by any operating aircraft. Usually, they start from an already flying baseline, making difficult the design of a completely new hybrid-electric aircraft without an initial conventional design. Aero-propulsive interactions aspects are carefully considered, since the installation of electric motors enable an easy setup of the Distributed Electric Propulsion (DEP), one of the main technologies improving overall aircraft performance [5–7], but the interdependence of the design parameters and the continuous update of the geometry as well as of the aerodynamic characteristics is neglected.

Thus, the first challenge to solve is having a design process that starts from a baseline defined only with the Top-Level Aircraft Requirements (TLAR). Such a pre-design is usually performed with statistical data on a conventional aircraft. Another challenge is a sound comparison between conventional and hybrid-electric or full-electric architectures, which is difficult to perform with a different design method for each architecture. By defining a single conceptual design process for conventional, hybrid-electric, and full-electric architecture, it will be possible to compare the weight breakdown in case of analogue design missions, where the power sources (fuel, batteries, fuel cells, and others) are sized with an energetic analysis of the mission profile. Such a method can be validated on conventional airplanes by comparing the results with available data on operating aircraft.

The conceptual design chain is described in Sec. III, highlighting the main structure of the present software. Section IV explains the power train modelling and architecture functionalities, whereas the overall detailed design process is summarized in Sec. V. Finally, in Sec. VI two different applications are described, highlighting main pros and cons of hybrid-electric aircraft configurations.

III. Conceptual Design Chain

The conceptual design aims to choose a single aircraft configuration, which suits the TLAR and aviation regulations requirements. In case of a hybrid-electric aircraft, it is important to explore different powertrain operating modes, which will be discussed in Sec. IV, with the mission profile to maximize the efficiency of the air transport. The conceptual design workflow is divided in three main modules: pre-design, sizing, and analysis, shown in Fig. 1. Such investigation may be included in an optimization loop targeting, for instance, minimum weight penalties, reduced emissions, and minimized DOC.

The preliminary design process moves from the statistical definition of the main geometrical characteristics depending on top-level requirements. It is a necessary step to have a baseline when designing a completely new aircraft. The following step is the sizing process, which starts after fixing the characteristics of the propulsive architecture in terms of geometry, hybridization parameters, and operating modes. The evaluation of aviation regulation constraints and mission requirements yield to the choice of the sizing point, that is the combination of wing loading W/S and power loading W/P. The last step is the analysis of the energetic requirements and flight performance, which is a crucial step in order to verify the compliance with aviation regulations and TLAR, and to optimize the aircraft.

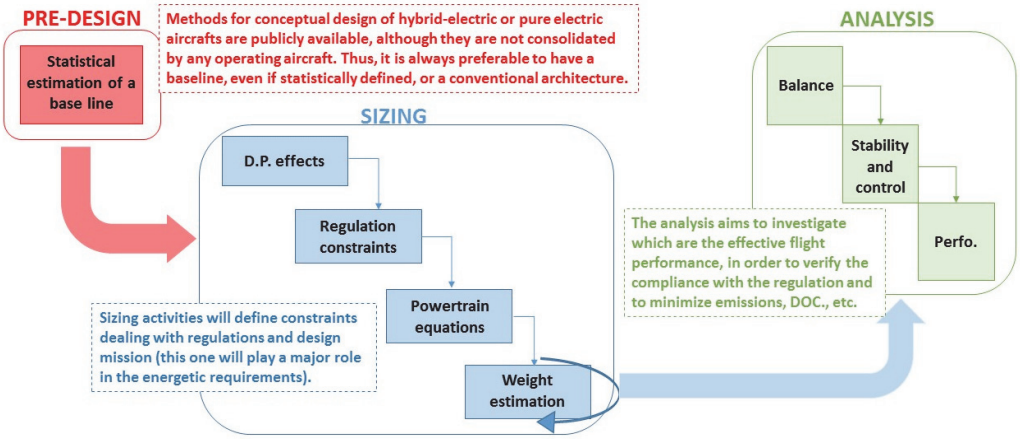

Fig. 1 Conceptual design process for a hybrid-electric aircraft.

IV. Propulsive architecture modeling

In the present work, the most general architecture considered includes two propulsive systems [8], as shown in Fig. 2. The Power Management And Distribution (PMAD) unit and the blue gearbox are the nodes that split the energy coming from different power sources (fuel, battery, etc.) on the two propulsive systems. Distributed propulsion, made possible by the size of electric

motors, is one of the main advantages of hybrid-electric architectures [9]. Here, "primary propulsive system" (colored blue in Fig. 2) refers to the propulsive units that are mainly powered from the thermal engine, whereas the thrust generators directly connected to the electric motors, like a DEP system, are addressed as "secondary propulsive system" (colored red in Fig. 2).

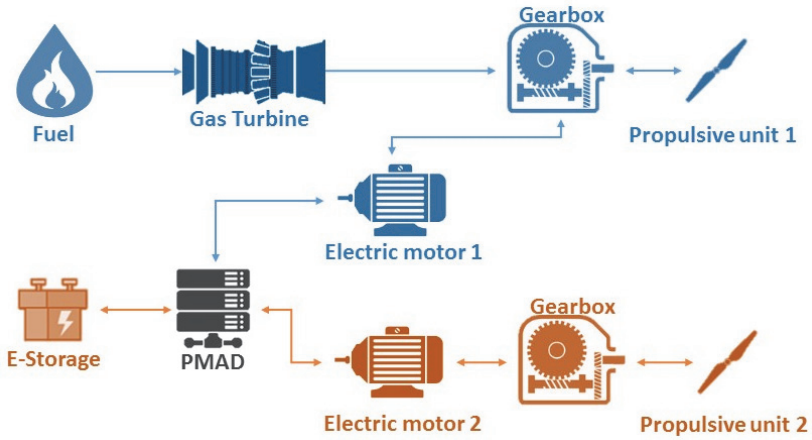

Fig. 2 The most general propulsive architecture considered in the present work.

Two different hybridization parameters are defined to cover a wide range of architectures. Both are based on power ratios: one is the ratio between the electric energy power source and total power source, named *supplied power ratio* Φ, the other is the ratio between secondary powertrain propulsive power and total propulsive power, named *shaft power ratio* φ [3]

$$\Phi = \frac{P_{\text{E-storage}}}{P_{\text{fuel}} + P_{\text{E-storage}}} \tag{1}$$

$$\varphi = \frac{P_{\text{prop 2}}}{P_{\text{prop 1}} + P_{\text{prop 2}}} \tag{2}$$

A third hybridization parameter, necessary to estimate the variation of the aerodynamic coefficients (ΔC_L, ΔC_{D_0} and ΔC_{D_i}), is defined as the ratio between the distributed thrust and the total thrust of the aircraft. Equation (3) relates this parameter to the shaft power ratio φ

$$\chi = \frac{1}{1 + \frac{\eta_{P1}}{\eta_{P2}}\left(\frac{1-\varphi}{\varphi}\right)} \tag{3}$$

however, the use of two thrust sources is only compatible with powertrain architectures that have two types of propulsive systems, otherwise Eq. (3) is undefined.

The powertrain operating mode is the power path from the energy source to propulsors. Operating modes may change during the mission. Nine operating modes will be considered for the presented architectures, as reported in Table 1 [1]. The number of independent combinations derives from the following considerations:

1) the gas turbine is a non-reversible component, transforming the fuel chemical energy into shaft power;
2) propellers may provide thrust or harvest power;
3) electrical machines may operate as motor or generator;
4) the electric energy source (e.g. battery) may be charged or discharged;
5) with the scheme of Fig. 2, the operating mode of electrical machine 2 depends on that of propulsive unit 2, electrical machine 1, and electric energy source.

Table 1. Hybrid-electric powertrain operating modes [1].

	1	2	3	4	5	6	7	8	9
P1	thrust	thrust	thrust	thrust	thrust	thrust	harvest	harvest	harvest
P2	thrust	thrust	harvest	thrust	harvest	harvest	thrust	thrust	harvest
E-Storage	discharge	charge	charge	discharge	discharge	charge	discharge	charge	charge
EM1	generator	generator	generator	motor	motor	motor	generator	generator	generator

V. Detailed conceptual design process

The design chain workflow is illustrated in Fig. 3. Each main box is described in the following sub-sections.

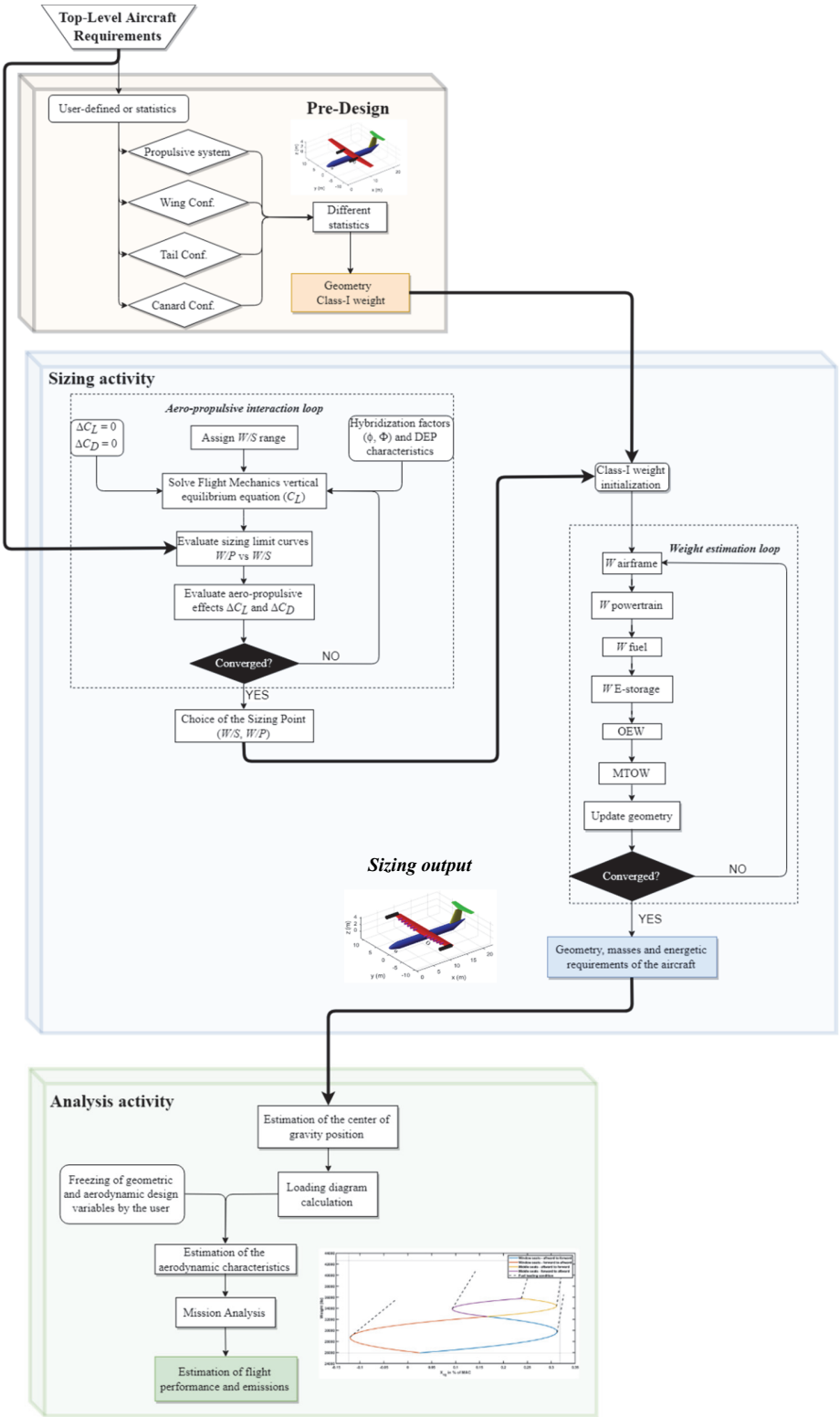

Fig. 3 Design chain workflow. The sizing module has been exploded.

A. Pre-Design activity

The predesign activity fills a gap between the conventional conceptual design methods and those available to design hybrid-electric aircrafts. The main objective is the definition of a baseline reference aircraft by querying response surfaces based on a wide range of aircraft geometrical parameters plotted with respect to top-level requirements and aircraft classification [10], or by applying semi-empirical correlations. The baseline will be defined by a complete set of geometrical and inertial parameters whose values will be changed according to designer free choices before starting the sizing activity. By assuming that a hybrid-electric or full-electric powertrain will not radically change fuselage and tail-plane for a conventional tube-and-wing configuration, statistical data will define the main layout of the airplane, including an initial step for weight estimation [11]. The fuselage, for example, is defined by the type of aircraft (e.g. a blended wing-body will have a different width with respect to a conventional fuselage), the number of passengers, and the position of the propulsive system. Other aircraft configurations, including non-conventional layouts as blended wing body or boxed wing for instance, may be added if statistical data or surrogate models are available.

Weight estimation, which usually is a direct calculation performed at the very beginning of the airplane design [11], is an iterative process performed in the sizing module to include both fuel and electric energy consumptions for a given mission profile. Different aircraft categories can be initialized referred to conventional aircraft: “Single Engine”, “Twin Engine”, “Regional Turboprop”, “Business Jet”, “Transport Jet”. Once the baseline aircraft has been initialized in the pre-design phase, an aircraft data structure is created (see Table 2), useful in the following sizing procedure. The Pre-design output structure is directly used in the following Sizing activities.

Table 2. Aircraft data structure.

Field	Sub-fields	Data	Attributes
TLAR	…	Value	Unit
Geometry	…	Value	Unit
Powertrain	…	Value	Unit
Weight	…	Value	Unit

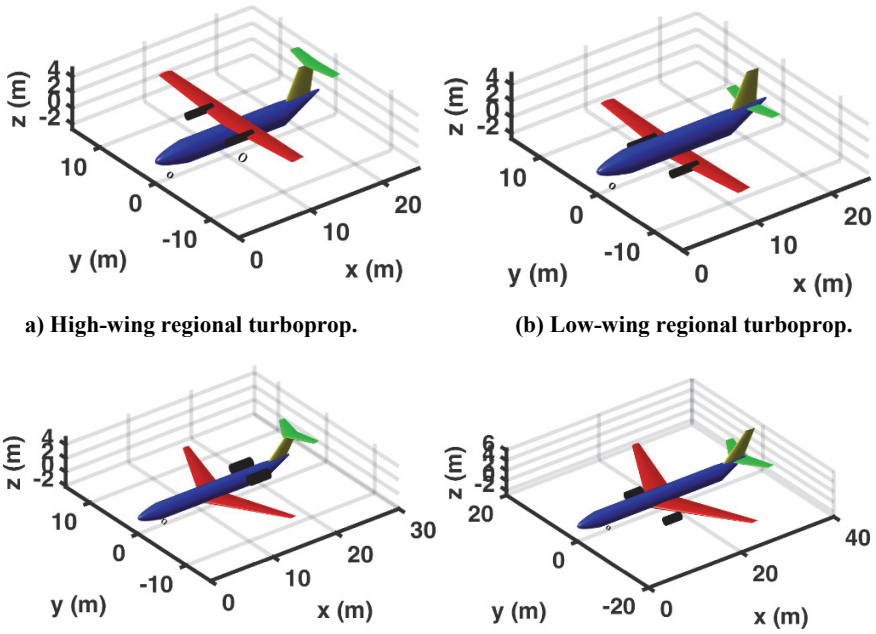

a) High-wing regional turboprop. **(b) Low-wing regional turboprop.**

(c) Business jet. **(d) Transport jet.**

Fig. 4 Some of the possible Pre-Design geometry data output.

B. Sizing activity – Preliminary evaluation of the aero-propulsive interactions

The sizing activity defines constraints due to aviation regulations and design mission and performs calculation on the aircraft sizing point (wing loading W/S and power loading W/P), powertrain sizing, and weight breakdown. The first step is the definition of the main parameters of the two propulsive systems. The geometry, the number of propulsive power sources, the hybridization factors, and the operating modes for each phase of the mission profile are the elements necessary to evaluate the interactions between the airframe and the propulsive system [1]. At this point of the design process, the evaluation of the interactions is limited to the effects of the propulsor, modelled as actuator disk, on the airframe [12,13]. The change in propeller efficiency due to the presence of the lifting surfaces is not considered [14]. According to Refs. [15,16], once a propeller geometry is assumed, it is expected an increase in efficiency and thrust due to the presence of the wing (propeller ahead of the wing). In particular, the upwash, due to the presence of the wing, induces both an uneven inflow on the propeller, resulting in an uneven disk loading, and a reduced

the axial velocity and angle of attack, compared to the freestream condition, resulting in an increase in thrust and efficiency. This increase is more pronounced in case of flap deflections. In case of DEP configuration, main variables are the diameter of the disk and the blade loading, which become also the limiting factors for the number of distributed propellers. As previously stated, the change in propeller efficiency due to the presence of the airframe is neglected, but its reduction with the increase of disc loading is included, as described later.

The interaction between the propulsive system and the main lifting surface is resumed by three main effects due to the increments of air pressure and speed through the actuator disk: the effect on the lift ΔC_L, the effect on the induced drag ΔC_{D_i}, and the effect on the zero-lift drag ΔC_{D_0}. The effect of the wake swirl is neglected.

The aerodynamic effects related to the interaction between the propeller wake and the lifting surfaces are part of an iterative process applied to the Flight Mechanics equilibrium equations. The method used to estimate the variation of the aerodynamic coefficients (ΔC_L, ΔC_{D_0} and ΔC_{D_i}) is based on the approach suggested by Patterson et al. [12]. The model assumptions can be resumed as follows:

1) the velocity increase at the actuator disk is computed assuming uniform axial inflow;
2) the variations of the aerodynamic coefficients due to swirl are neglected;
3) the flow over the wing has no separation;
4) the airfoil is symmetric;
5) the effect of each propeller on the adjacent ones is neglected;
6) the effect of the propellers on the wing is uniform and limited to the area covered by distributed propulsion;
7) the wing area influenced by distributed propulsion is fully immersed in propeller slipstream, half of which flows under the wing and half over the wing.

Under these assumptions, this method is mainly valid for clean configurations [12]. Its application in configurations with flaps deployed is useful as a first approximation in the conceptual design phase.

The distributed propulsion is analyzed with three geometrical parameters describing the position and the distribution of the propulsive system and the propeller disks. Independently from the geometry, the wing is considered rectangular, since there is no reason to increase complexity when the concept has not been frozen. Thus, the wing is described by two main geometric parameters: the span, *b*, and the chord, *c*. According to Fig. 5, the distributed propulsion system is characterized by *N* propellers (*N/2* propellers per semi-span) of diameter D_P. The parameter $\Delta y/b$ represents the wing span fraction occupied by distributed propulsion, δ_y the gap between the propellers in percentage of propeller disk diameter, and x_p/c is the axial position of the propeller disk from the leading edge in unit chord. The thrust line of secondary propulsors is at an angle α_p with respect to freestream velocity. The angle i_p between the propeller disk axis and the wing chord represents the incidence of the propeller. Finally, the angle between the wing chord and the freestream velocity is the angle of attack α.

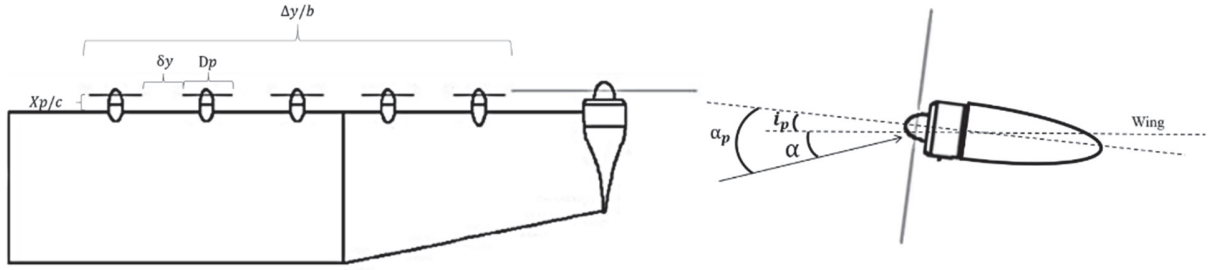

Fig. 5 Geometrical scheme of a wing with distributed propulsion and tip-mounted engine.

The aerodynamic coefficients variation is estimated by Eqs. (4), (7), and (8). In particular, the increase in wing section lift coefficient due to the increment in local freestream velocity is computed as follow:

$$\Delta c_l = 2\pi \left[\left(\sin\alpha - a_{c/4}\beta \sin i_p \right) \sqrt{(a_{c/4}\beta)^2 + 2a_{c/4}\beta \cos\left(\alpha + i_p\right) + 1} - \sin\alpha \right] \tag{4}$$

where β is a finite-slipstream correction factor, estimated with the surrogate model proposed in [12], and $a_{c/4}$ is the axial induction factor at the quarter of the chord. Since during the sizing process the angle of attack of the wing is unknown, it can be estimated using the three-dimensional lift coefficient generated by the only airframe aerodynamics [5]:

$$\alpha \simeq \frac{C_L}{2\pi AR} \left[2 + \sqrt{AR^2(1-M^2) + \left(1 + \frac{\tan^2(\Lambda_{c/2})}{1-M^2}\right) + 4} \right] \tag{5}$$

where *AR* is the wing aspect ratio, *M* is the freestream Mach number, and $\Lambda_{c/2}$ is the wing half-chord sweep angle. Thus, this approach assumes that the aircraft with DEP is flying at the same angle of attack of the aircraft with conventional powertrain.

Variations of the aerodynamic coefficients are used later to size the wing including the effects of distributed propulsion. The variation in drag coefficient is estimated as the sum of two contributions:

$$\Delta c_d = \Delta c_{d0} + \Delta c_{di} \tag{6}$$

the first term is estimated as a function of the skin friction coefficient c_f, whereas the second one is a function of the lift coefficient and the aspect ratio

$$\Delta c_{d0} = a_{c/4}^2 \, c_f \tag{7}$$

$$\Delta c_{di} \simeq \frac{2 C_{L_{\text{airframe}}} \Delta c_l}{\pi A} \tag{8}$$

It is here highlighted that by applying the simple method presented above to evaluate the increase in aerodynamic coefficients, the benefit of distributed propulsion will be underestimated. In fact, the method does not consider the enormous advantage given by the presence of energized flow moving through slotted flaps or in presence of high curvature.

The obtained two-dimensional coefficients are multiplied for the wing surface fraction S_{DEP}/S_w affected by distributed propulsion to obtain the variation of three-dimensional aerodynamic coefficients. These aerodynamic effects enlarge the design space allowing a larger wing loading in landing configuration.

C. Sizing activity – Calculation of the aircraft sizing point

The curves in Fig. 6 show the differences between the sizing plot of an ATR-42 in case of conventional and hybrid-electric powerplant. The constraint curves of the sizing plot, in absence of DEP, are a function of aviation regulations (FAR 25 aircraft) as well as aircraft minimum performance requirements (e.g. balanced field length). The enabling of DEP moves these constraints. The combination of hybridization factors and operating modes is such that a significant increment in landing wing loading limit value is allowed with distributed propulsion, with a negligible effect in cruise and some of the climb conditions. Details on the application are given in Sec. VI.

The sizing plot is the framework in which the designer chooses the raw properties of the aircraft: wing loading *W/S* and power loading *W/P*. Each limit curve is calculated through an iterative process for each flight phase, using the equilibrium condition along the z-axis of the aircraft and sweeping over a given range of wing loadings *W/S*. A loop of three steps is repeated until convergence to tolerance (changes in "deltas" between two consecutive steps below 0.1%), as shown in Fig. 7:

1) estimation of the lift coefficient by z-axis equilibrium condition (9) for each wing loading of the sizing plot range, where C is the rate of climb, q_∞ is the dynamic pressure and μ is the ramp angle.

$$C_{L_{\text{airframe}}} = \frac{\frac{W}{S}\sqrt{1-\left(\frac{C}{V}\right)^2} - \chi \frac{T}{W} \sin\alpha_p \cos\mu}{q_\infty \cos\mu} - \Delta C_L \tag{9}$$

2) estimation of the power loading *W/P* in each mission phase based on the constraint equations [11];
3) estimation of the aero-propulsive interaction between DEP and airframe in term of "deltas" of the aerodynamic coefficients to apply in Eq. (9) for the following iterative step.

At convergence, the values of power loading are plotted with the corresponding values of wing loading for each phase.

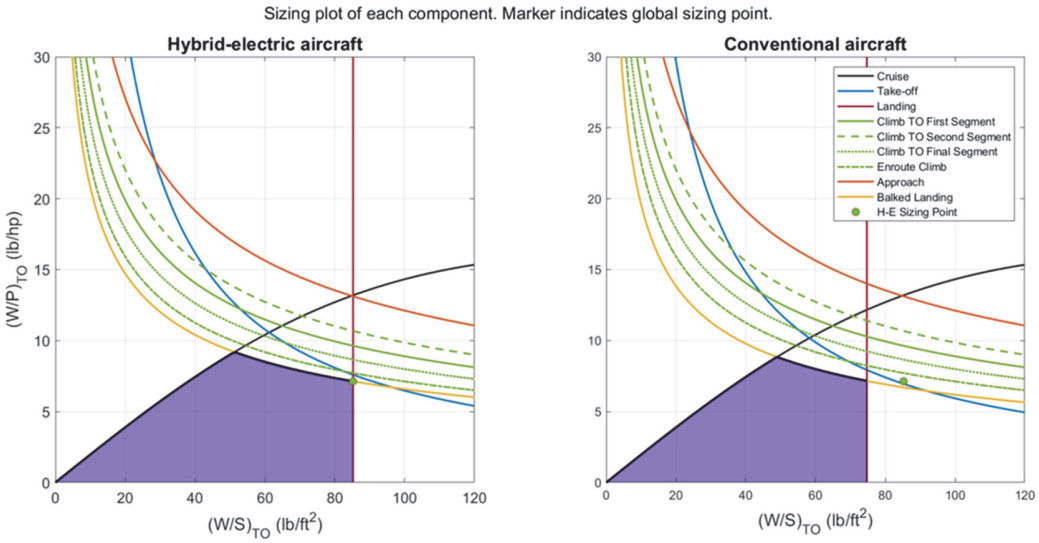

Fig. 6 Sizing plot curves comparison for both hybrid-electric and conventional powertrain.

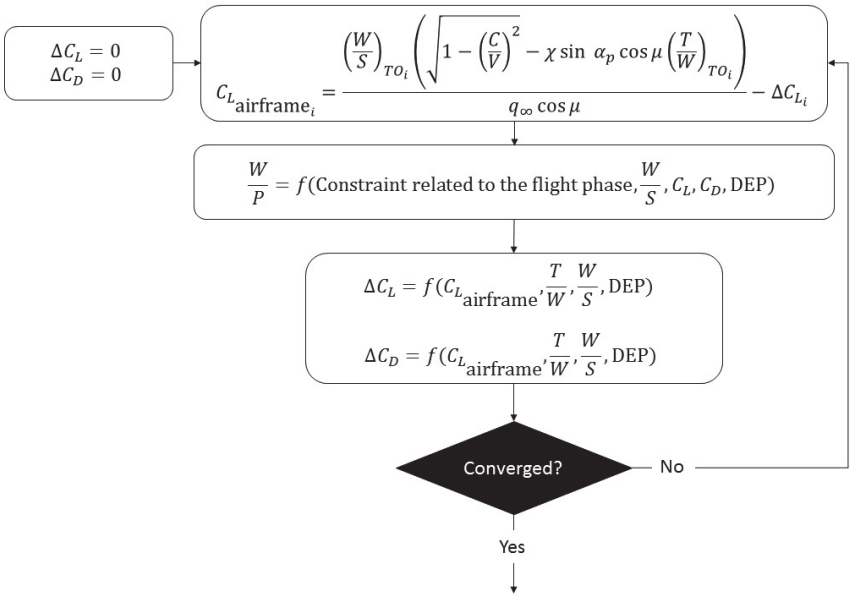

Fig. 7 Loop for the evaluation of the aero-propulsive interaction.

D. Sizing activity – Powertrain equations

The choice of the sizing point depends on the design objectives (low emissions, low battery weight, minimum DOC, etc). Once the sizing point is chosen, the single components of the propulsive system are sized using a system of ten equations: seven equations based on the energy balance for each component and three equations based on the hybridizations factors to close the system [1]. An example of such a system, written for operating mode 1 (refer to Table 1), is reported in Eq. (10). It is a mathematical representation of the power path and split from the energy sources to the propulsive units, hence defining the sizing requirements for each powertrain component.

By assuming that an operating mode is constant for each mission phase, i.e. the matrix coefficients is constant, although its elements may vary for each mission phase, Eq. (10) is a linear system. The unknowns array represents the power required by each powertrain component to satisfy the total propulsive power (right-hand side) with the assigned efficiencies and hybridization parameters (matrix coefficients).

At this stage, the weight of the hybrid-electric aircraft is unknown, as well as the required total power. Thus, the equations system (10) is written with the inverse of the power loading *P*/*W* and it is solved for each mission phase. The sizing point of each component is calculated as the most power-demanding (highest *P*/*W* value) among those calculated for each mission phase. To get the sizing plot charts of each component, as reported in Fig. 8, system (10) is also solved for each constraint curve of the sizing plot, where the known term is varied to cover all the power loading values of each constraint curve of the aircraft sizing plot chart.

$$\begin{bmatrix} -\eta_{GT} & 1 & 0 & 0 & 0 & 0 & 0 & 0 & 0 & 0 \\ 0 & -\eta_{GB} & 1 & 1 & 0 & 0 & 0 & 0 & 0 & 0 \\ 0 & 0 & 0 & -\eta_{P1} & 0 & 0 & 0 & 0 & 1 & 0 \\ 0 & 0 & -\eta_{EM1} & 0 & 1 & 0 & 0 & 0 & 0 & 0 \\ 0 & 0 & 0 & 0 & -\eta_{PM} & -\eta_{PM} & 1 & 0 & 0 & 0 \\ 0 & 0 & 0 & 0 & 0 & 0 & -\eta_{EM2} & 1 & 0 & 0 \\ 0 & 0 & 0 & 0 & 0 & 0 & 0 & -\eta_{P2} & 0 & 1 \\ \Phi & 0 & 0 & 0 & 0 & (\Phi-1) & 0 & 0 & 0 & 0 \\ 0 & 0 & 0 & \varphi & 0 & 0 & 0 & (\varphi-1) & 0 & 0 \\ 0 & 0 & 0 & 0 & 0 & 0 & 0 & 0 & 1 & 1 \end{bmatrix} \cdot \begin{bmatrix} P_f \\ P_{gt} \\ P_{gb} \\ P_{s1} \\ P_{e1} \\ P_{bat} \\ P_{e2} \\ P_{s2} \\ P_{p1} \\ P_{p2} \end{bmatrix} = \begin{bmatrix} 0 \\ 0 \\ 0 \\ 0 \\ 0 \\ 0 \\ 0 \\ 0 \\ 0 \\ P_{TO} \end{bmatrix} \tag{10}$$

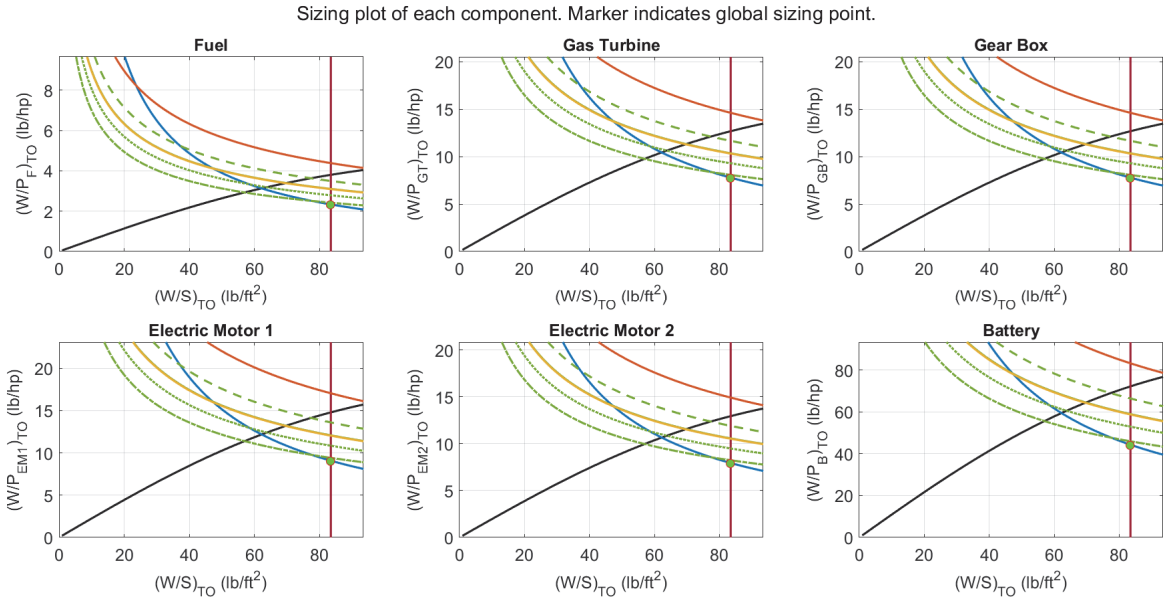

Fig. 8 Sizing plots of different powertrain components.

E. Sizing activity – Weight estimation

The final step of the sizing activity is the weight estimation. The maximum take-off weight of the aircraft is calculated as

$$W_{TO} = W_{OE} + W_{\text{payload}} + W_{\text{fuel}} + W_{\text{E-storage}} \tag{11}$$

$$W_{OE} = W_{\text{airframe}} + W_{PT} + W_{\text{crew}} \tag{12}$$

where:

W_{OE} is the operative empty weight, which is split in three contributions: airframe, powertrain, crew
W_{airframe} is the weight of the structures, including equipment, but except powertrain, calculated with a Class-II method [17]
W_{PT} is the weight of the powertrain calculated with Eq. (11)
W_{crew} is the weight of the crew, calculated with a Class-I method [11]
W_{payload} is the weight of the payload, calculated with a Class-I method [11]
W_{fuel} is the weight of the fuel, calculated from mission analysis
$W_{\text{E-storage}}$ is the weight of the electric energy storage (e.g. batteries)

Preliminary weight estimation for an aircraft with conventional powertrain is a smooth process, where fuel weight is calculated with Breguet formulas [11]. For a non-conventional powertrain, the determination of the weight of the energy sources may not be straightforward, since they depend on several factors, including the required power and energy profile, which in turn depend on the aircraft weight. Moreover, the powertrain is no more treated as a single component, but as a system where power is split across its subsystems according to the operating mode, hybridization factor, and components technology (efficiency). Although a modified Breguet formula for hybrid-electric aircraft has been proposed [3], here the weight estimation is performed as an iterative process to implement a mission-oriented method that is almost independent from energy source, following the approach of Ref. [1].

The aircraft weight is initiated with a Class-I method [11] assuming a conventional powertrain, i.e. with only primary engines. This provides the weight of payload and crew, which is fixed for any powertrain, and a first guess for the operative empty weight, fuel, and max take-off weight, and it is performed on Pre-design activities. The alternative energy sources are not considered in the initialization.

The weight estimation loop is illustrated in Fig. 9. To get an accurate estimate, assuming that the non-conventional powertrain does not radically changes the aircraft structure and equipment, a Class-II weight method [17] is used for the airframe. Powertrain weight is calculated from the solution of Eq. (10), which includes operating mode, hybridization factors, and technology level (component efficiency in power transformation or split), together with the specific power of each component and the take-off weight calculated in the previous step. As done with the powertrain equations, the most limiting (i.e. heavy) result for each component is taken to the next step. Then, fuel and electric energy storage weights are calculated with the analysis of the mission energetic profile, by assuming constant power for each mission phase. This calculation will be more accurate in the analysis module, where the mission is analyzed step by step and geometrical characteristics of the aircraft have been frozen. As regard the alternative energy source weight, this is calculated as the max value between the energetic approach and the powertrain equations (10) output (i.e. by power or by energy required). Finally, all the contributions are summed and, when the difference between the take-off weights of the last two iterations is below a given threshold ε, the loop is considered converged and output values are provided. In Table 5, the results of this approach are reported for three different powertrain architectures.

The iterative procedure for the estimation of the weights drives an update of geometry as well. In fact, to be compliant with the chosen sizing point, the wing area and span are updated, hence an update of the propeller disks diameter is performed to be compliant with the chosen percentage of wing span blown by the propellers. This operation may change the maximum efficiency of the propellers and, thus, an update of the design space. For similar reasons related to tail volumetric coefficient, an update of the tail geometry is required. Therefore, the sizing activity should be considered iterative and the convergence criterion is evaluated on difference of DEP disk diameter between iterations. At the update of the geometry of the wing and propulsors diameter, the propeller efficiency is evaluated again with momentum theory [20]. As previously stated, the propeller is modelled as an actuator disk, which is a circular surface of zero thickness characterized by a pressure jump accelerating the air through the disk. The actuator disk theory provides the maximum theorical efficiency achievable.

The thrust T of the propeller can be calculated with both Eq. (13) and Eq. (14)

$$T = \rho V_{as}(V_{as} - V_\infty)A_s \tag{13}$$

$$T = \Delta p A_p \tag{14}$$

where V_{as} is the velocity far downstream, where the pressure has returned to the environment value, ρ is the flow density, assumed constant, A_s is the cross-sectional area of the slipstream, A_p is the disk area, and Δp is the pressure increment through the disk. The pressure jump can be described in terms of speed with Eq. (15)

$$\Delta p = \frac{1}{2}(V_{as}^2 - V_\infty^2) \tag{15}$$

Since the continuity equation ensures that $A_s V_{as}$ is equal to $A_p V_p$, where V_p is the speed on the propeller disk, it is possible to combine Eq. (14) and Eq. (15) in Eq. (16)

$$V_p = \frac{1}{2}(V_{as} + V_\infty) \tag{16}$$

Considering the power, as calculated by Eq. (17), it is possible to substitute the values of power required and available thrust in Eq. (18) to obtain Eq. (19), which has been used in the iterative process to check and propeller efficiency at any phase: if propeller efficiency is equal or lower than the initial, user-defined value, η_p is updated, otherwise the initial value is kept in the calculation

$$P = \frac{1}{2}\rho V_{ap}(V_{as}^2 - V_\infty)A_p \tag{17}$$

$$\eta_p = \frac{TV_\infty}{P} \tag{18}$$

$$\eta_p = \frac{2}{1+\sqrt{1+\frac{T}{\frac{1}{2}\rho V_\infty^2 A_p}}} \tag{19}$$

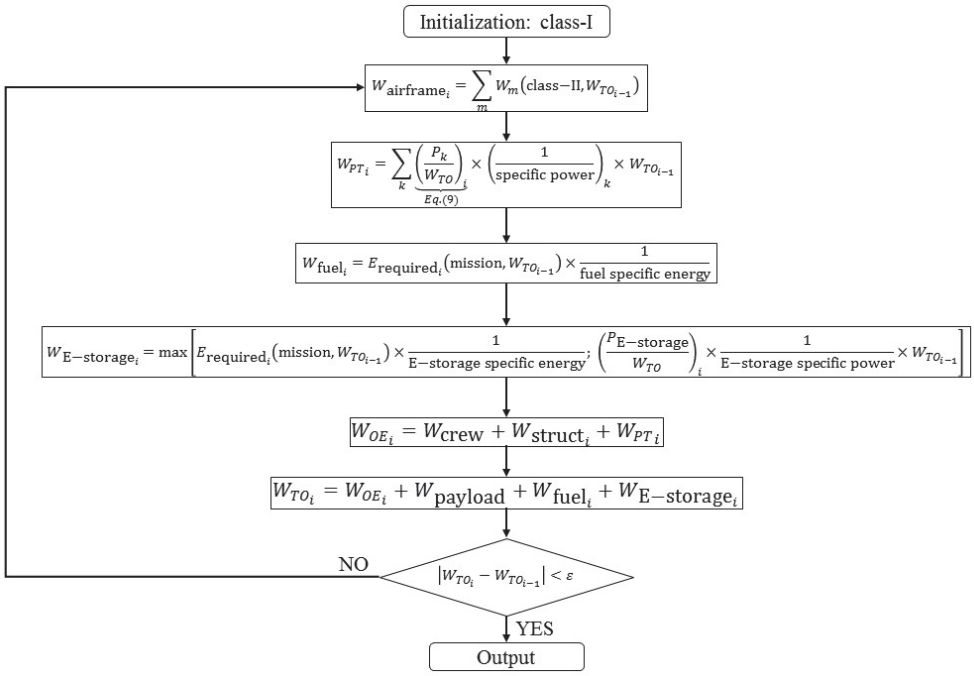

Fig. 9 Weight estimation loop.

The workflow for the weight estimation highlights the importance of both power density and energy density when studying the secondary power source depending on the choice of the range or the power supplying strategy. In fact, for certain requirements, it could lead to a dimensioning activity based on energy, due to longer time of use of secondary power source. Otherwise, if the mission profile requires a lower energy supplying performance, the aircraft is sized at the maximum required power (usually at take-off). In this second case the power peak value is the critical parameter for the sizing of the secondary power source.

The eligible concepts to size should be chosen carefully to limit the so-called weight snowball effect. In fact, since the first iteration starts by adding the unconventional powertrain elements, as, for example, batteries or electric motors, the following iteration starts by redefining the weights which depends on the new maximum take-off weight, as, for example, the undercarriage whose strength and weight depends on the maximum take-off weight to sustain. If the TLAR are too demanding for the technology level chosen (i.e. specific power and energy), the iterative weight estimation diverges.

F. Analysis activity

The analysis aims to investigate the effective flight performance and check the compliance with aviation regulations and design objectives. The tool part required to perform the analysis provides a baseline to the subsequent optimization. The analysis is performed in three different steps. The first step aims to provide a more accurate estimation of the interactions between the propulsive system and the airframe. The second one provides a high-fidelity analysis of the mission profile energetic requirements by using the efficiency polynomial laws of the powertrain elements and an accurate breakdown of the mission phases. The last step deals with the estimation of the emissions that is the key parameter to minimize when designing a hybrid-electric aircraft.

The analysis concludes the loop guiding the choice of the best concept. This will be the baseline for the multi-objective optimization module. For the sake of brevity, the steps of the performance analysis will be described in detail in a future paper, focusing here on the first two steps, Pre-Design and Sizing.

G. Semi-automatic report generation

Although not included in the workflow, the developed tool can generate a human-readable report in a semi-automatic way. The initial effort in writing the code and standard text paragraphs is payed-off with the possibility to get a formatted PDF document with data and figures, allowing the designer to focus on the results of his concepts with a high quality, presentation-ready report.

VI. Application

A. Preliminary results for different hybridization factors

The assessment of the results is a crucial step in order to minimize the number of analyses and test cases for the consequent optimization. Table 3 summarizes the top-level requirements, derived from the available ATR-42 data. Before proceeding to the analysis of hybrid-electric aircrafts, it is advisable to compare the conventional concept fulfilling the same requirements and the hybrid-electric concepts sized with different hybridization percentages. Aircraft configurations underpinning the applications are shown in Fig. 10, a conventional high-wing-engine configuration and a DEP configuration, with wing tip-mounted gas-turbine (GT). In principle, GT engines can be located anywhere the user wants. The tool computes the available wingspan to locate DEP propellers based on wing dimension, GT and DEP propeller diameters, and the number of DEP motors (see again Fig. **5** for clarity).

Several concepts are explored choosing the values of the design parameters in a wide range, considering both turbo-electric and hybrid-electric aircraft concepts, always starting from a conventional configuration used as baseline for the comparison. The importance of this preliminary selection has been already highlighted, thus, in the present section the objective is to show the high variability of the objective functions to minimize and of the main output variables of interest. Moving from the TLAR listed in Table 3 and the characteristics of electric components in Table 4 [19], the analysis of the different concepts is operated changing the number of distributed propellers and the value of the different hybridization factors. In this section, a constant value of the hybridization factor has been assigned at each mission phase where DEP has been enabled, but this strategy can be changed to investigate different combinations. The maximum take-off weight and the operative empty weight evaluated in case of concepts with unconventional powerplants are bigger than in case of conventional concepts, due to the higher number of powertrain components. Thus, the chosen figure of merit for a sound comparison of the different aircraft configurations is the fuel weight. The exploration of the possible concepts aims to identify the set of design variables guaranteeing a lower fuel consumption for a given mission, yielding to a cleaner aircraft.

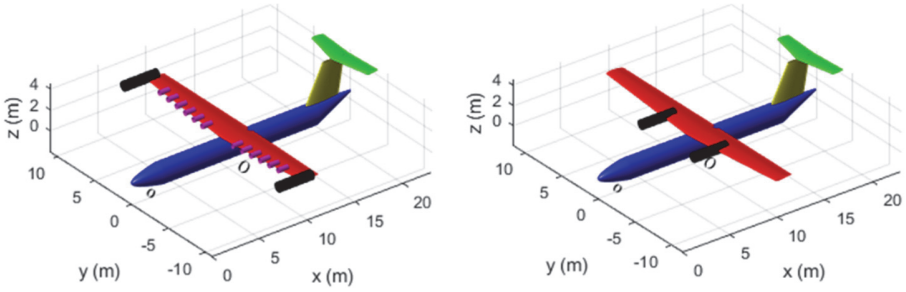

Fig. 10 Examples of two different aircraft concepts with and without distributed propellers.

Table 3. TLAR (ATR-42).

	Value
Number of passengers	48
Design range	840 nm
Landing field length	3600 ft
Take-off field length	4000 ft
Mach number – cruise	0.47
Cruise altitude	17000 ft
Alternate range	200 nm
Fuel reserve	5%
Holding	30 min
Number of primary engines	2

Table 4. Characteristics of the electric elements.

	Value
Specific Energy of the Battery (Wh/kg)	500
Specific Power of the Battery (kW/kg)	1.0
Energy Density (Wh/l)	800
Specific Power of the EM (kW/kg)	7.7
Number of DEP engines	Variables
Wing span covered by DEP $\Delta y/b$	0.60
Gap between DEP props δ_y (unit D_p)	0.01

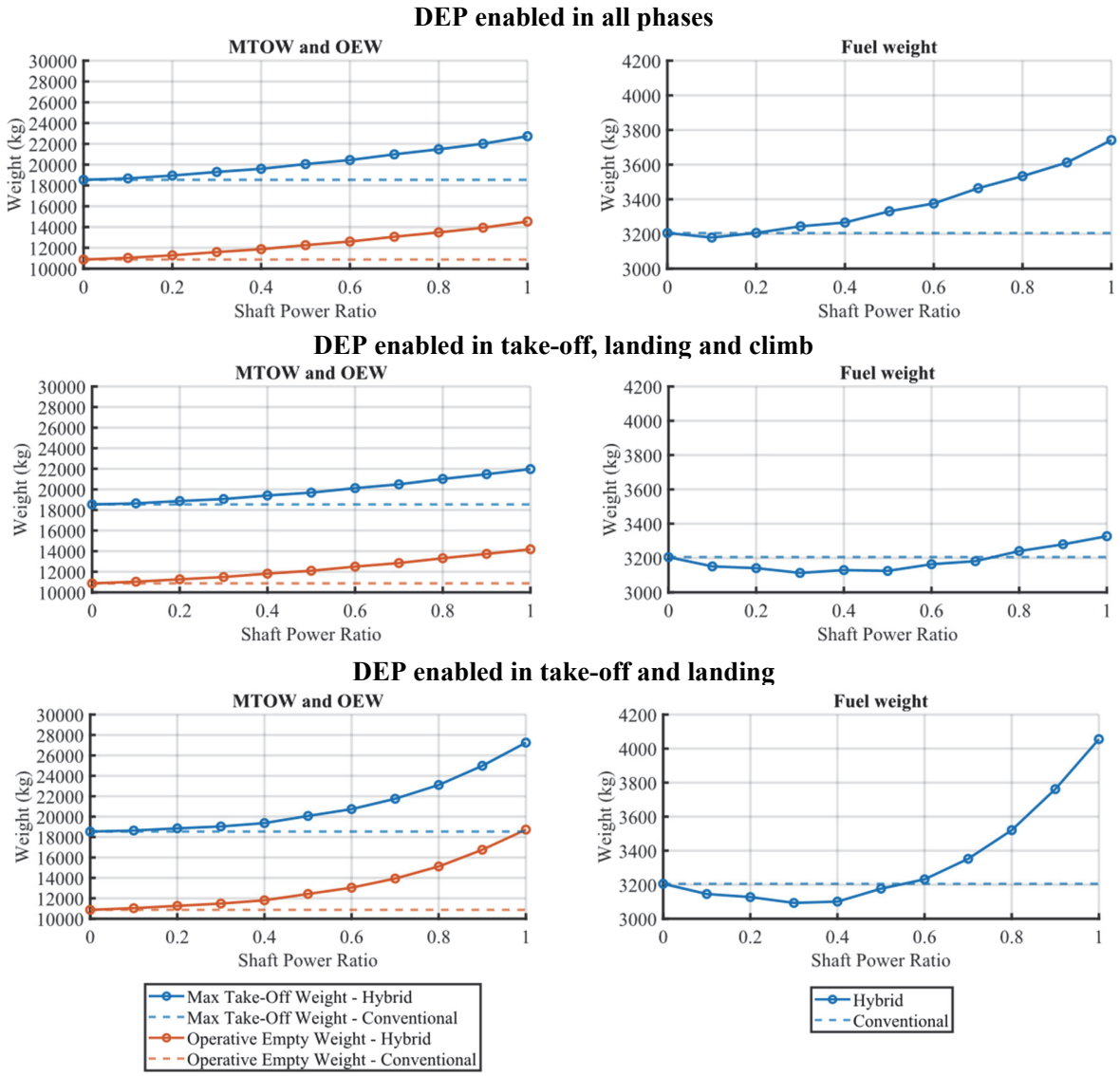

Fig. 11 Weights comparison for a turboelectric aircraft with different usage strategy of 20 distributed propellers.

All the investigated design concepts with hybrid-electric powertrain have the gas turbines with the primary propellers installed on the wingtips and the secondary distributed propulsors covering the inner 60% of the wingspan, with 1% diameter gap between propellers. A possible design concept has DEP enabled at take-off and landing only, without a secondary energy source. Such a configuration is known as turbo-electric. The choice of this mission strategy about the use of DEP is explained in Fig. 11, which is

an excerpt of a larger numerical analysis dataset. The use of distributed propulsion in all phases other than short phases (e.g. take-off and landing) does not yield to a fuel saving, due to the additional mechanical losses extended over time and undesired increase of drag. DEP is used for lift augmentation, not to provide thrust, therefore its benefits in cruise are lost. On the other hand, at low values of φ the effect can be mitigated with a low percentage of hybridization of supplied power, as detailed subsequently.

Even when this limit is imposed, there is a high variability of the aerodynamic coefficients to consider due to the presence of a different number of distributed propellers. The higher the thrust provided by the single propeller is, the higher will be the blowing perceived by the wing, but this effect is influenced by the number of propellers. In fact, when the number of propellers increase, the disk diameter decreases. Consequently, the disc loading increases for a given thrust, limiting the maximum propeller efficiency. In Fig. 12 it is shown that operating the same subdivision of the total thrust, or, in other words, flying at the same value of φ, a higher lift coefficient increment is obtained in case of a higher number of distributed propellers. The same trend is observed for the drag coefficient.

In Fig. 13, the secondary power source is introduced and enabled, as well as for DEP, at take-off and landing. The figure shows that, for a wide range of shaft power ratio φ and number of distributed propellers, the presence of the battery is a disadvantage, due to its lower specific energy with respect to the fuel. The same figure highlights the importance of choosing carefully the mission profile and the shaft power ratio provided by the secondary propulsive system. In fact, at constant supplied power ratio Φ and TLAR, the fuel weight reduction is maximized at a precise value of the shaft power ratio. The technological level chosen is resumed by the factors provided in Table 4, from Ref. [19].

However, this consideration made about the supplied power ratio cannot be applied at any other mission profile or DEP enabling strategy and, conversely, the consideration made about the advantages deriving from employing DEP only at take-off and landing, or in general in short time flight phases, cannot be seen as a general recommendation on the use of the secondary power source. In case of activation in short flight phases, the power peak is the sizing factor for designing the power source. On the contrary, when the secondary power source is employed in long time phases, the energy to supply to the propulsive system becomes the sizing factor. This is the reason why no reliable assumptions can be made about the best strategy for the use of electric energy storage unit regardless of TLAR and DEP. What has been stated identifies the boundary of the design space analyzed in the present work:

1) DEP is analyzed for a wide range of shaft power ratios φ, but the use is limited at take-off and landing;
2) The supplied power ratio Φ is analyzed for a wide range of values considering two different possible strategies: the first one considering the use of secondary power unit at take-off and landing and whose results are synthetized in Fig. 13, the second one considering Φ > 0 in all phases except for the cruise, whose long range would make the energy requirements prohibitive, Fig. 14.

The hybrid electric aircraft concepts require an overview of the limits linked to the use of batteries or other electric power sources when there is a coupling between the two hybridization factors. In case of secondary power source enabled at take-off and landing only, the higher is Φ, the higher will be the fuel consumption. This can be explained considering that the power required from the battery is higher increasing Φ and the electric power source is fundamentally an inert mass for the most part of the flight mission when this strategy is employed. On the contrary, when a secondary power source is activated during long range phases, the effect of the fuel reduction has a major impact with respect to the increase of energetic requirements due to the higher weight. The two flight strategies are compared in Fig. 15.

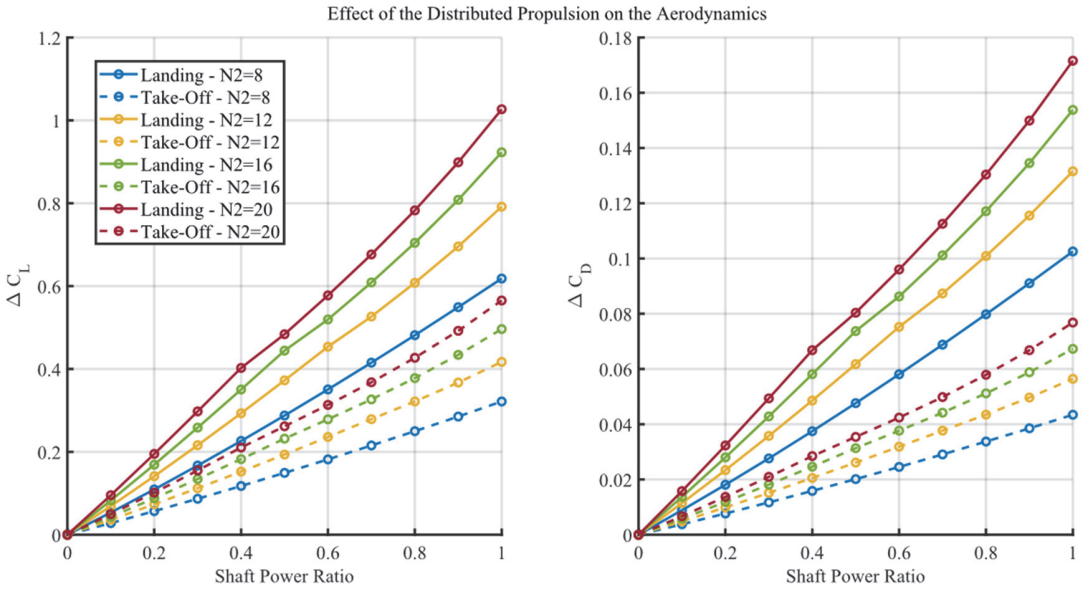

Fig. 12 Effects of DEP on lift and drag coefficients at different φ and Number of Distributed Propellers.

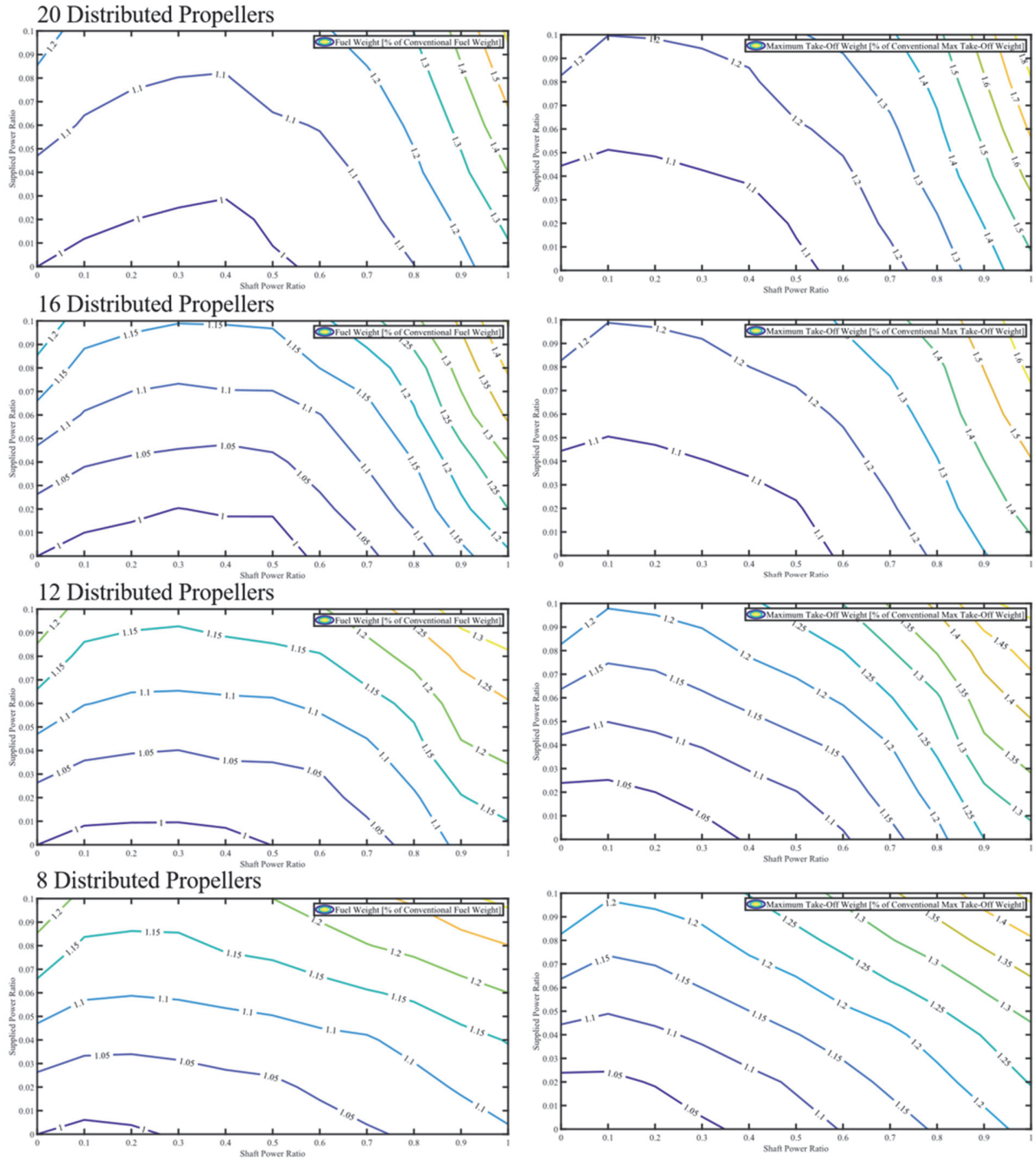

Fig. 13 Contour plot of the ratio of fuel weight and maximum take-off weight with respect to supplied and shaft power ratios for different number of distributed propellers. $\varphi > 0$ and $\Phi > 0$ at take-off and landing (840 nm).

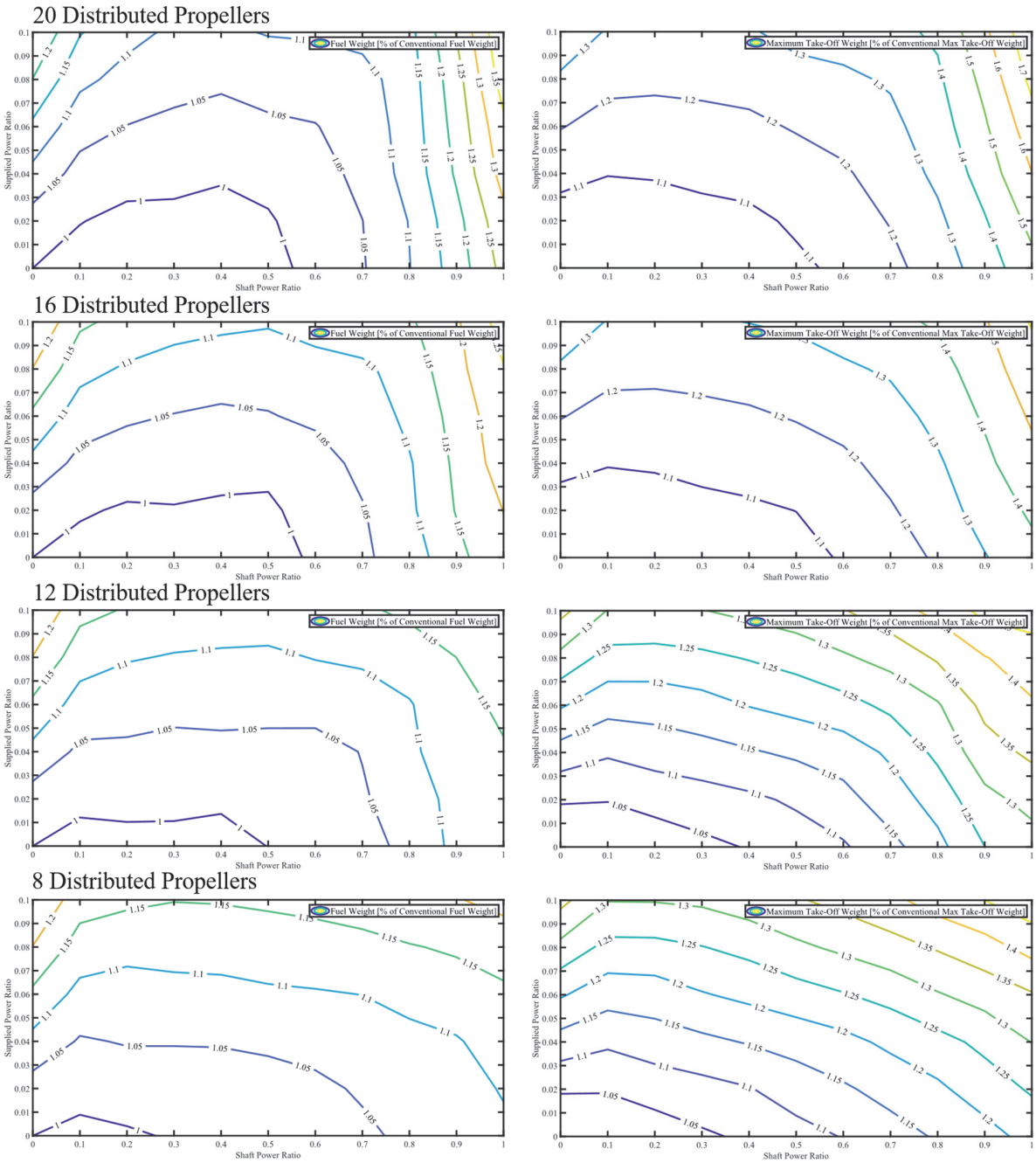

Fig. 14 Contour plot of the ratio of fuel weight and maximum take-off weight with respect to supplied and shaft power ratios for different number of distributed propellers. $\varphi > 0$ at take-off and landing only, $\Phi > 0$ in all phases except for cruise (840 nm).

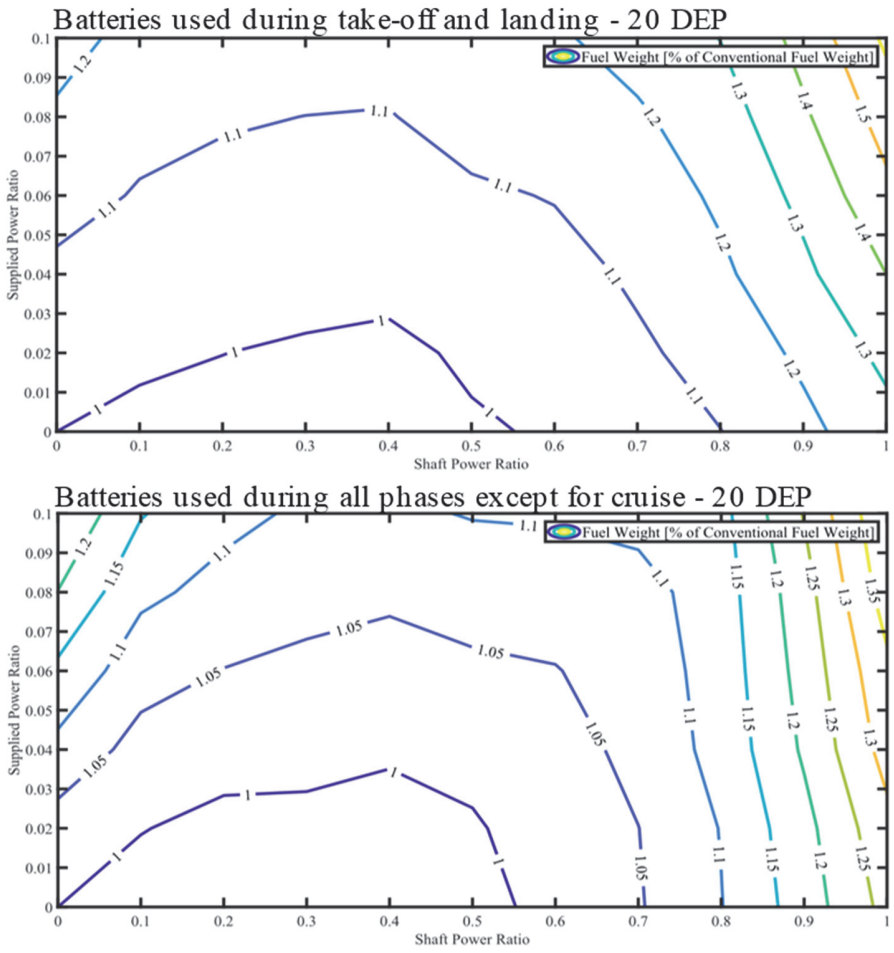

Fig. 15 Contour plot of the ratio of fuel weight change with respect to supplied and shaft power ratios for the two flight strategies presented (secondary propulsive system with 20 distributed propellers).

B. Application results for the proposed TLAR

The assessment of the results is a crucial step to minimize the number of analyses and test cases for the consequent optimization. Moving from the sizing of the possible concepts, it is possible to choose a single configuration to analyze. In the present case, 540 different configurations[*] have been analyzed with MATLAB® limiting the range of design variables to the hybridization factors and the number of distributed propellers. The sizing activity of each configuration needs 8 seconds. In the end, considering the minimization of the fuel weight as main objective of the design activity, the configuration chosen is the turboelectric concept number 2, with 20 distributed propellers and the 40% of power provided by the secondary propulsive system ($\varphi = 0.40$) at take-off and landing.

Table 5 provides an overview of both distributed propulsion main characteristics and sizing results. The higher weight due to the low specific energy of the battery is one of the main challenges for the future. On the other hand, turboelectric aircraft, which does not have a secondary power source, can be considered as a possible alternative to conventional concepts.

The results dealing with hybrid-electric concepts in Table 5 stress the necessity of running different simulations with different hybridization strategy along the flight mission to maximize the benefits. In fact, the comparison between the two airplanes highlights how the increase in maximum take-off weight is not directly connected to an increase of fuel consumption. In the same way, the two compared turbo-electric aircraft stress the importance of choose carefully the DEP operating strategy, since a stronger aero-propulsive interaction connected to a higher thrust provided by the secondary propulsive system is not directly connected to better flight performance. The importance of excluding those missions where the hybridization factors give disadvantages is related to the computational charge of the optimization tool. The last column opens a design path towards a concept characterized by distributed propulsion used in landing and take-off conditions, with no secondary electric power source. Thus, after checking the accuracy of the sizing activity results, moving from this comparison the analysis and optimization could be limited to one concept.

[*] Configurations analyzed in a design sweep on a pc Intel i7 2.3 GHz, 8Gb RAM – 8 seconds/configuration working on 1 core.

Table 5. Summary of the application of the sizing tool on a regional turboprop with different powertrains.

	ATR-42*	Conventional	Hybrid-electric 1	Hybrid-electric 2	Turboelectric 1	Turboelectric 2
Operating modes						
Take-off	1	1	1	1	1	1
Climb	1	1	4	1	1	1
Cruise	1	1	1	1	1	1
Loiter	1	1	4	1	1	1
Alternative cruise	1	1	4	1	1	1
Descent	1	1	4	2	1	1
Landing	1	1	1	1	1	1
Hybridization parameters						
Φ - Take-off	0	0	0.02	0.02	0	0
Φ – Climb	0	0	0.02	0	0	0
Φ – Cruise	0	0	0.02	0	0	0
Φ – Loiter	0	0	0	0	0	0
Φ – Alternate cruise	0	0	0.02	0	0	0
Φ – Descent	0	0	0.02	0	0	0
Φ – Landing	0	0	0.02	0.02	0	0
φ – Take-off	0	0	0.40	0.40	0.60	0.40
φ – Climb	0	0	0	0	0	0
φ – Cruise	0	0	0	0	0	0
φ – Loiter	0	0	0	0	0	0
φ – Alternate cruise	0	0	0	0	0	0
φ – Descent	0	0	0	0	0	0
φ – Landing	0	0	0.40	0.40	0.60	0.40
DEP inputs and effects						
No. of motors	0	0	20	20	20	20
$\Delta y/b$	0	0	0.60	0.60	0.60	0.60
δ_y	0	0	0.01	0.01	0.01	0.01
$\Delta C_{L\ \text{landing}}$	-	0	0.40	0.40	0.58	0.42
$\Delta C_{L\ \text{take-off}}$	-	0	0.21	0.21	0.32	0.22
Geometry						
Wing area (m^2)	54.48	50.81	47.76	47.10	46.82	46.21
Weight breakdown (kg)						
Max take-off mass	18600	18538	20022	19745	20737	19370
Zero fuel mass	-	15333	16884	16595	17505	16269
Operative empty mass	11200	10869	12421	12131	13042	11806
Fuel mass	-	3205	3138	3150	3232	3101
Battery mass	-	-	521	383	-	-
Powertrain mass	-	2280	3070	3020	3991	3130
Wing mass	-	1188	1241	1212	1250	1188
Horizontal tail mass	-	219	163	151	150	147
Vertical tail mass	-	211	157	158	156	153
Fuselage mass	-	2080	2080	2080	2080	2080
Energy breakdown (kWh)						
Battery energy†	-	-	208	3.22	-	-
Fuel energy	-	36633	35868	35997	36934	35437

Table 6. 200 nm, typical mission TLAR for hybrid-electric regional aircraft.

	Value
Number of passengers	48
Design range	200 nm
Landing field length	3600 ft
Take-off field length	4000 ft
Mach number – cruise	0.47
Cruise altitude	17000 ft
Alternate range	30 nm
Fuel reserve	5%
Holding	15 min
Number of primary engines	2

* As declared on the ATR website: http://www.atraircraft.com

† Assuming a battery specific energy of 500 Wh/Kg.

The results dealing with TLAR on which the previous analysis is based could be considered unsatisfactory since only the 3% of fuel can be saved considering the present-day technologies. However, when considering a disruptive technology, it is appropriate to investigate new application and, so, new requirements. In the present case the comparison has been performed with respect to a baseline, ATR-42, whose TLAR are particularly unfavorable in case of hybrid-electric aircrafts. Considering the typical range of ATR-42, a completely different design mission has been proposed to investigate the sensitivity of these new technologies to the mission profile. The TLAR proposed are listed in Table 6.

Table 7. Comparison of the characteristics of a conventional aircraft and a full electric aircraft

	Conventional	Hybrid-electric	Full-electric
Operating modes			
Take-off	1	1	4
Climb	1	4	4
Cruise	1	4	4
Loiter	1	4	4
Alternative cruise	1	4	4
Descent	3	2	2
Landing	1	1	4
Hybridization parameters			
Φ - Take-off	0	0.50	1.00
Φ – Climb	0	0.50	1.00
Φ – Cruise	0	0.50	1.00
Φ – Loiter	0	0.50	1.00
Φ – Alternate cruise	0	0.50	1.00
Φ – Descent	0	0.50	1.00
Φ – Landing	0	0.50	1.00
φ – Take-off	0	1.00	1.00
φ – Climb	0	0	0
φ – Cruise	0	0	0
φ – Loiter	0	0	0
φ – Alternate cruise	0	0	0
φ – Descent	0	0	0
φ – Landing	0	1.00	1.00
DEP inputs and effects			
Number of engines	0	20	20
$\Delta y/b$	0	0.60	0.60
δ_y	0	0.01	0.01
$\Delta C_{L\ \text{landing}}$	0	1.03	1.03
$\Delta C_{L\ \text{take-off}}$	0	0.56	0.56
Geometry			
Wing area [m^2]	40.22	63.42	98.85
Weight breakdown [kg]			
Max take-off mass	14675	31938	48773
Zero fuel mass	14050	31692	48773
Operative empty mass	9587	27229	44309
Fuel mass	625	245	0
Battery mass	-	10824	21040
Powertrain mass	1849	4608	6999
Wing mass	1024	2267	3990
Horizontal tail mass	117	264	576
Vertical tail mass	121	273	596
Fuselage mass	2080	2080	2080
Energy breakdown [kWh]			
Battery energy*	-	2802	6287
Fuel energy	7144	2802	0

The aircraft designed moving from these requirements cannot be compared to the previous conventional baseline, thus, the first analysis performed aims to investigate the characteristics of a completely new baseline. The analysis is again performed for a wide range of hybridization factors. What is particularly remarkable is that the energetic requirements are not prohibitive as they were in the previous case and that, except for high shaft power ratios and for supplied power ratios $\Phi < 5\%$, when the power requirements are higher than energetic requirements, the presence of the battery is always enormously advantageous, as shown in Fig. 16. Figure 17 shows the maximum take-off weight ratio with respect to conventional maximum take-off weight. In Table 7 the results dealing with the full-electric aircraft are compared to the conventional concept designed on the same mission profile. The technological level considered is the same previously considered (see again Table 4), but the shorter mission range opens to a more efficient use of both batteries and DEP. Fuel saving is more than 50% when switching to a hybrid-electric powertrain with 50%

* Assuming a battery specific energy of 500 Wh/Kg.

propulsive power provided by batteries in all flight phases and DEP enabled at take-off and landing. Yet, the maximum take-off weight is more than doubled for the hybrid-electric configuration and more than three times bigger for the full-electric aircraft. Increments for the operating empty weight are even bigger, with 284% for the hybrid-electric and 462% for the full-electric configuration. It must be noted that, considering a battery volume density of 800 Wh/l at cell level [19], decreasing this value by 5% for packaging level, the full electric configurations will need of about 8 cubic meters for battery storage, that is about the overall baggage compartment for an ATR42[†].

It is here remarked that comparisons cannot be performed considering the same operating modes on a wide range of hybridization factors, since there is a strong coupling among the three parameters. For example, when DEP is disabled, the battery should provide energy to the primary propulsive system. In this situation, the electric machine 1 in Fig. 2 cannot work as generator, hence the operating mode is changed from 1 to 4 (see again the description in Table 1). In the same way, for full-electric concepts some operating modes are not available, as for example, operating mode 1. Thus, the designer must be aware of how the propulsive system works from the very beginning of the sizing activity.

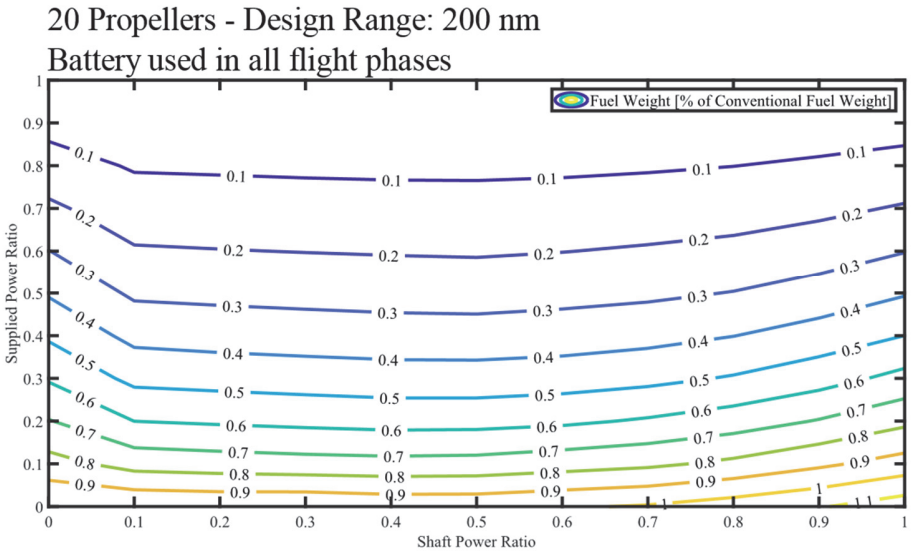

Fig. 16 Contour plot of the ratio of fuel weight with respect to supplied and shaft power ratios (secondary propulsive system with 20 distributed propellers).

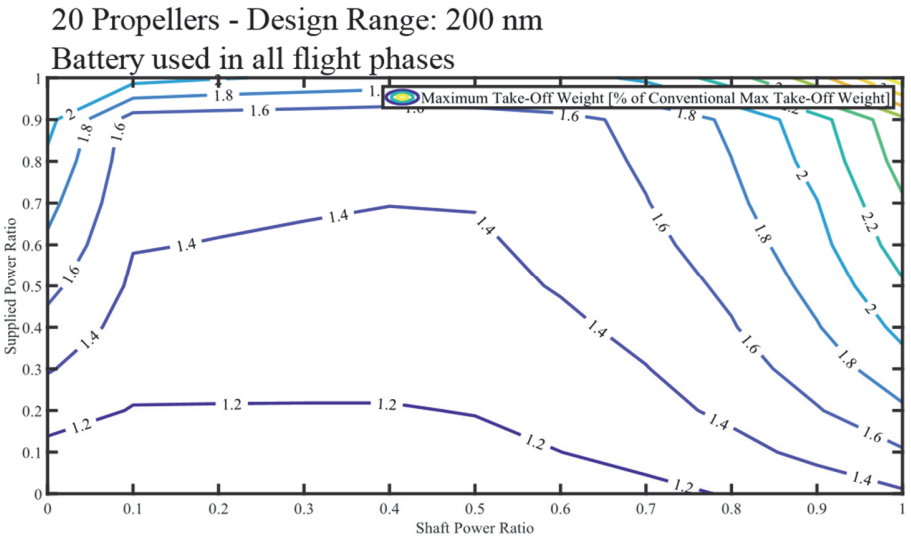

Fig. 17 Contour plot of the ratio of maximum take-off weight with respect to supplied and shaft power ratios (secondary propulsive system with 20 distributed propellers).

[†] As declared on the ATR website: http://www.atraircraft.com

VII. Conclusion

The present paper defines a workflow for the aircraft and its single components preliminary sizing, which is an implicit and necessary step in case of hybrid-electric and turbo-electric aircrafts. The design workflow is unique and suitable for hybrid-electric, turbo-electric, and conventional concepts. The design activity moves from statistics correlations between TLAR and geometry, then, after the sizing activity, the geometry and the weights are updated. In the end, the analysis of the fuel required for the design mission is the driving factor for the choice of the baseline of a possible optimization. Results from the sizing activity based on a wide range of design variables have been discussed. The actual findings show that, with the actual technology, a regional turboprop with a turbo-electric powertrain and distributed propulsion is comparable in terms of weight and fuel consumption to the conventional aircraft. Improvements are foreseen with a more accurate interaction between the wing aerodynamics and the airflow induced by DEP in high lift conditions, where the air blowing on a slotted flap may significantly increase the lift coefficient.

Considering also that the TLAR are the same of the ATR-42, which is already optimized for its mission, it is apparent that with the actual technology level there is little possibility for a different powertrain to be advantageous. However, noise and emissions may be lower in take-off and landing conditions with DEP enabled. By considering future trends in energy storage, the hybrid-electric powertrain may become more attractive. Finally, an optimization on the driving parameters of the sizing activity may reveal some improvements with the state-of-the-art technology and may even suggest a variation of the mission profile.

Acknowledgments

This research work has been inspired and partly financed by the Italian PROSIB (Propulsione e Sistemi Ibridi per velivoli ad ala fissa e rotante – Hybrid Propulsion and Systems for fixed and rotary wing aircraft) project PNR 2015-2020 lead by Leonardo S.p.A.

References

[1] de Vries, R., Brown, M.T., and Vos, R., "A Preliminary Sizing Method for Hybrid-Electric Aircraft Including Aero-Propulsive Interaction Effects," in: *2018 Aviat. Technol. Integr. Oper. Conf.*, No. June, 2018. doi:10.2514/6.2018-4228.c1.

[2] Strack, M., Pinho Chiozzotto, G., Iwanizki, M., Plohr, M., and Kuhn, M., "Conceptual Design Assessment of Advanced Hybrid Electric Turboprop Aircraft Configurations," in: *17th AIAA Aviat. Technol. Integr. Oper. Conf.*, American Institute of Aeronautics and Astronautics, Reston, Virginia, June 2017. doi:10.2514/6.2017-3068.

[3] Voskuijl, M., van Bogaert, J., and Rao, A.G., "Analysis and design of hybrid electric regional turboprop aircraft," *CEAS Aeronautical Journal*, Vol. 9, No. 1, 2018. doi:10.1007/s13272-017-0272-1.

[4] Antcliff, K.R., Guynn, M.D., Marien, T. V., Wells, D.P., Schneider, S.J., and Tong, M.T., "Mission Analysis and Aircraft Sizing of a Hybrid-Electric Regional Aircraft," January 2016.

[5] Deere, K.A., Viken, J.K., Viken, S., Carter, M.B., Wiese, M., and Farr, N., "Computational Analysis of a Wing Designed for the X-57 Distributed Electric Propulsion Aircraft," in: *35th AIAA Appl. Aerodyn. Conf.*, American Institute of Aeronautics and Astronautics, Reston, Virginia, No. June, 2017. doi:10.2514/6.2017-3923.

[6] Viken, J.K., Viken, S., Deere, K.A., and Carter, M., "Design of the Cruise and Flap Airfoil for the X-57 Maxwell Distributed Electric Propulsion Aircraft," in: *35th AIAA Appl. Aerodyn. Conf.*, No. June, 2017: pp. 1–41. doi:10.2514/6.2017-3922.

[7] Della Vecchia, P., Malgieri, D., Nicolosi, F., and De Marco, A., "Numerical analysis of propeller effects on wing aerodynamic: tip mounted and distributed propulsion," *Transportation Research Procedia*, Vol. 29, January 2018. doi:10.1016/J.TRPRO.2018.02.010.

[8] Felder, J.L., "NASA Electric Propulsion System Studies Outline," *NASA Presentation*, November 2018.

[9] *Commercial Aircraft Propulsion and Energy Systems Research*, The National Academies Press, Washington, DC, 2016. doi:10.17226/23490.

[10] Torenbeek, E., *Advanced Aircraft Design : Conceptual Design, Technology and Optimization of Subsonic Civil Airplanes.*, Wiley, 2013.

[11] Roskam, J., *Airplane design*, DARcorporation, Lawrence, Kan, 2000.

[12] Patterson, M.D., Daskilewicz, M.J., and German, B., "Simplified Aerodynamics Models to Predict the Effects of Upstream Propellers on Wing Lift," in: *53rd AIAA Aerosp. Sci. Meet.*, American Institute of Aeronautics and Astronautics, Reston, Virginia, January 2015. doi:10.2514/6.2015-1673.

[13] Marcus, E.A., de Vries, R., Raju Kulkarni, A., and Veldhuis, L.L., "Aerodynamic Investigation of an Over-the-Wing Propeller for Distributed Propulsion," in: *2018 AIAA Aerosp. Sci. Meet.*, American Institute of Aeronautics and Astronautics, Reston, Virginia, January 2018. doi:10.2514/6.2018-2053.

[14] Veldhuis, L.L.M., "Propeller Wing Aerodynamic Interference," 2005.

[15] Sinnige, T., van Arnhem, N., Stokkermans, T.C.A., Eitelberg, G., and Veldhuis, L.L.M., "Wingtip-Mounted Propellers: Aerodynamic Analysis of Interaction Effects and Comparison with Conventional Layout," *Journal of Aircraft*, November 2018. doi:10.2514/1.C034978.

[16] Bass, R.M., "Small scale wind tunnel testing of model propellers," in: *24th AIAA Aerosp. Sci. Meet.*, American Institute of Aeronautics and Astronautics, Reno, NV, January 1986. doi:10.2514/6.1986-392.

[17] Torenbeek, E., *Synthesis of subsonic airplane design: an introduction to the preliminary design, of subsonic general aviation and transport aircraft, with emphasis on layout, aerodynamic design, propulsion, and performance*, Delft University Press, Delft, 1982.